Propagation of a femtosecond pulse in a microresonator visualized in time

H. Gersen, D. J. W. Klunder, J. P. Korterik, A. Driessen, N. F. van Hulst, and L. Kuipers*

Department of Science and Technology and MESA+ Research Institute, University of Twente, P.O. Box 217, 7500 AE Enschede, The Netherlands

Received January 20, 2004

A noninvasive pulse-tracking technique has been exploited to observe the time-resolved motion of an ultrashort light pulse within an integrated optical microresonator. We follow a pulse as it completes several round trips in the resonator, directly mapping the resonator modes in space and time. Our time-dependent and phase-sensitive measurement provides direct access to the angular group and phase velocity of the modes in the resonator. From the measurement the coupling constants between the access waveguides and the resonator are retrieved while at the same time the loss mechanisms throughout the structure are directly visualized.

OCIS codes: 250.5530, 170.5810, 170.6920, 120.3180, 320.2250.

The trapping of light within microresonators allows the storage of optical power and is important in a wide range of fields including (bio)sensing, nonlinear optics, and photonics.[1–4] Light is confined by total internal reflection inside the structure, and, whenever the optical path length of a round trip is equal to an integral number of wavelengths, a resonance mode is excited. Depending on geometry, these modes consist of chaotic and (or) stable orbits, such as bow-tie-shaped or whispering-gallery modes[2] (WGMs). WGMs have been directly visualized in microspheres[5] and in their integrated optics equivalent, the microresonator.[6,7]

However, in all cases, only the steady-state behavior of the light propagation was visualized. To date, time-dependent studies of WGMs have been limited to investigation of the output characteristics[8] or to a sophisticated pump–probe technique that yields insight into the round-trip time.[9] Recently, we showed that femtosecond pulses can be tracked in space and time while propagating through a waveguide.[10,11] In this Letter we exploit this technique to image for the first time to our knowledge the motion of an ultrashort optical pulse through a microresonator.

The device under study, fabricated in Si_3N_4 on SiO_2 technology,[12] is illustrated in Fig. 1. Simulations show that, of the two supported resonator modes (TE_{00} and TE_{01}), the TE_{01} mode is slightly affected by the inner rim. Although the TE_{00} mode is not affected by the inner rim and could be considered a quasi-WGM, this is not the case for the TE_{01} mode. We therefore designate these modes as resonator modes (RMs) rather than as WGMs. Light couples into the resonator through input waveguide WG1 and can couple out of the resonator into WG2. Local optical measurements are possible with a photon scanning tunneling microscope (PSTM). In the PSTM a small fraction of the evanescent field above the waveguiding structure is picked up with an uncoated subwavelength fiber probe (Fig. 1). To visualize dynamic effects inside the ring resonator, we launched femtosecond pulses ($\lambda = 1300$ nm, FWHM $= 123 \pm 2$ fs) into WG1. The PSTM signal is interferometrically mixed with part of the same pulse that has propagated along the reference branch. Heterodyne detection of the interference signal allows a separation of amplitude and phase information.[11]

Figure 2 shows the results of a PSTM measurement on both a high- [Figs. 2(a)–2(c)] and low-finesse [Figs. 2(d)–2(f)] resonator. The topography of the ring-shaped resonators, with a radius of 25 μm and a height of 300 nm, is presented in Figs. 2(a) and 2(d). Figures 2(b) and 2(e) show the time-resolved optical amplitude. In each measurement pulse envelopes are clearly visible at several positions in the device. Comparison of the amplitude in WG1 with the amplitude in the ring shows that more power is coupled to the low-finesse resonator [Fig. 2(e)] than to the high-finesse resonator [Fig. 2(b)]. This is to be expected as the level of coupling increases when the gap size decreases.[12,13] Figures 2(c) and 2(f) show the wave fronts of the circling RMs (arrows indicate location). Close inspection of the phase image clearly shows singularities due to interference of multiple RMs in the resonator.[14] The total number of fringes in the ring is a direct measure for the averaged

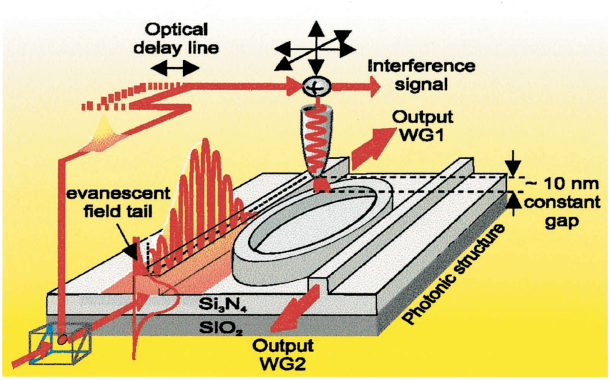

Fig. 1. Schematic overview of pulse tracking in a microresonator. The evanescent field of a pulse traveling inside the device is picked up by a fiber probe. At each position the signal picked up by the probe is interferometrically mixed with part of the same pulse that has propagated through the reference branch. The position of a delay line in the reference branch defines a reference time.

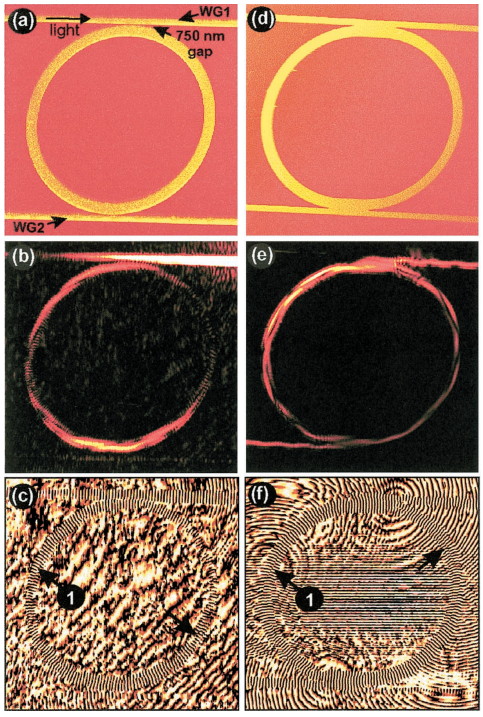

Fig. 2. PSTM images (65.7 μm $\times$ 65.7 μm) of two ring resonators: (a)–(c) device with an air gap of 750 nm; (d)–(f) device with no air gap; (a), (d) topography; (b), (e) time-resolved optical amplitude; (c), (f) cosine of the optical phase. The spatial beating pattern demonstrates the excitation of multiple RMs. Since the individual wave fronts of the RMs are visible in Figs. 2(c) and 2(e), counting the wave fronts in the ring combined with the wavelength difference given by the beating pattern suffices to determine an angular phase velocity of 7.24 and 7.54 rad/ps for the TE_{00} and TE_{01} RMs, respectively.

angular phase velocity, whereas the separation between subsequent singularities yields the difference in phase velocity for the modes. Combination of these numbers yields phase velocities of 7.24 rad/ps and 7.54 rad/ps for the TE_{00} and TE_{01} modes, respectively.

At the angular position of a singularity [indicated by 1 in Figs. 2(c) and 2(f)] the phase difference between the RMs is equal to π. As the phase difference between the RMs is known for this angular position, we can write the coupling between WG1 and the resonator as

$$E_{\mathrm{WG1}} = \kappa_{\mathrm{TE}_{00}}\left[\mathrm{TE}_{00} - \left(\frac{\kappa_{\mathrm{TE}_{01}}}{\kappa_{\mathrm{TE}_{00}}}\right)\mathrm{TE}_{01}\right], \qquad (1)$$

where κ is the coupling constant between the power-normalized mode in WG1 (E_{WG1}) and the respective power-normalized RMs (TE_{00} and TE_{01}). Instead of a direct comparison of optical amplitudes, the use of power-normalized modes guarantees power conservation. Fitting a sum of the mode profiles in the ring to the measured amplitude at the angular position of a singularity yields $\kappa_{\mathrm{TE}_{01}}/\kappa_{\mathrm{TE}_{00}}$ [see Eq. (1)]. Comparison with the amplitude of the incoming single-mode pulse in WG1 then yields the coupling coefficients for each individual mode. For the low-finesse device we find 33.5 $\pm$ 0.1% and 26.7 $\pm$ 0.1% for the TE_{00} and TE_{01} modes, respectively. A similar approach for the coupling to WG2 fails as two modes are excited in WG2. However, when neglecting the multimodal behavior in WG2, we see that 33 $\pm$ 0.4% of the mode in WG1 is coupled from WG1 to WG2 through the resonator. For the high-finesse device we find coupling coefficients of 0.9 $\pm$ 0.3% and 1.1 $\pm$ 0.3% for the TE_{00} and TE_{01} modes, respectively. A closer examination of the optical phase in the coupling region shows more differences between the two devices. When the air gap is open [Fig. 2(c)], we observe two separate wave fronts in the ring and WG1. A slight phase mismatch is observable. However, when the air gap is closed, the phase fronts are no longer separated. The spherical waves in Fig. 2(f), such as the ones originating at the coupling junctions, show that strong scattering occurs at these positions. This effect that is not observed for the high-finesse device.

Figure 3 shows snapshots of the measured optical amplitude from an ultrashort pulse as it couples into the ring and then completes two round trips in the low-finesse device. This device allows us to visualize both the pulses in the ring and outcoupled pulses on the same scale. Between each measurement, the reference time is shifted 200 $\pm$ 2 fs. Time stepping is started from the moment the pulse initially couples to the resonator [Fig. 3(a)]. A small fraction of the pulse propagating in WG1 is coupled into the resonator. In the sequence in Figs. 3(a)–3(l) the pulse travels around the ring, coupling energy out to the two adjacent waveguides at each pass. This results in a series of output pulses with diminishing amplitude at the output ports of WG1 and WG2, yielding a direct measure for the losses of the resonator. However, the coupling constants between the cavity and the waveguides are so large that the observed reduction in amplitude is completely dominated by the coupling losses. Figure 3(m) shows the position of the center of mass (CoM) in WG1 (red line) and WG2 (green line), which directly yields group velocities of (1.28 $\pm$ 0.02) $\times$ 10^8 and (1.33 $\pm$ 0.02) $\times$ 10^8 m/s in the respective waveguides. Because the observed pulses are roughly Gaussian, the CoM is given by the location of the maximum amplitude.[11] Figure 3(n) shows the angular position of the CoM of the pulse inside the resonator as a function of angular coordinates while neglecting the multimodal behavior. We find an averaged angular group velocity of 6.0 $\pm$ 0.2 rad/ps, which is in good agreement with the calculated values of 6.24 and 6.35 rad/ps for the supported RMs.

The propagation of femtosecond pulses in resonator modes of a microresonator has been studied both spatially resolved and in the time domain. We have visualized the optical amplitude and phase of a femtosecond pulse inside a microresonator. The visualization in time of a pulse propagating in a resonator yields the angular phase and group velocity of RMs independent of any model. The observed beating pattern in the resonator shows that multiple RMs have been excited. Comparison of the amplitudes in the resonator and waveguides yields the coupling coefficient between waveguides and resonator.

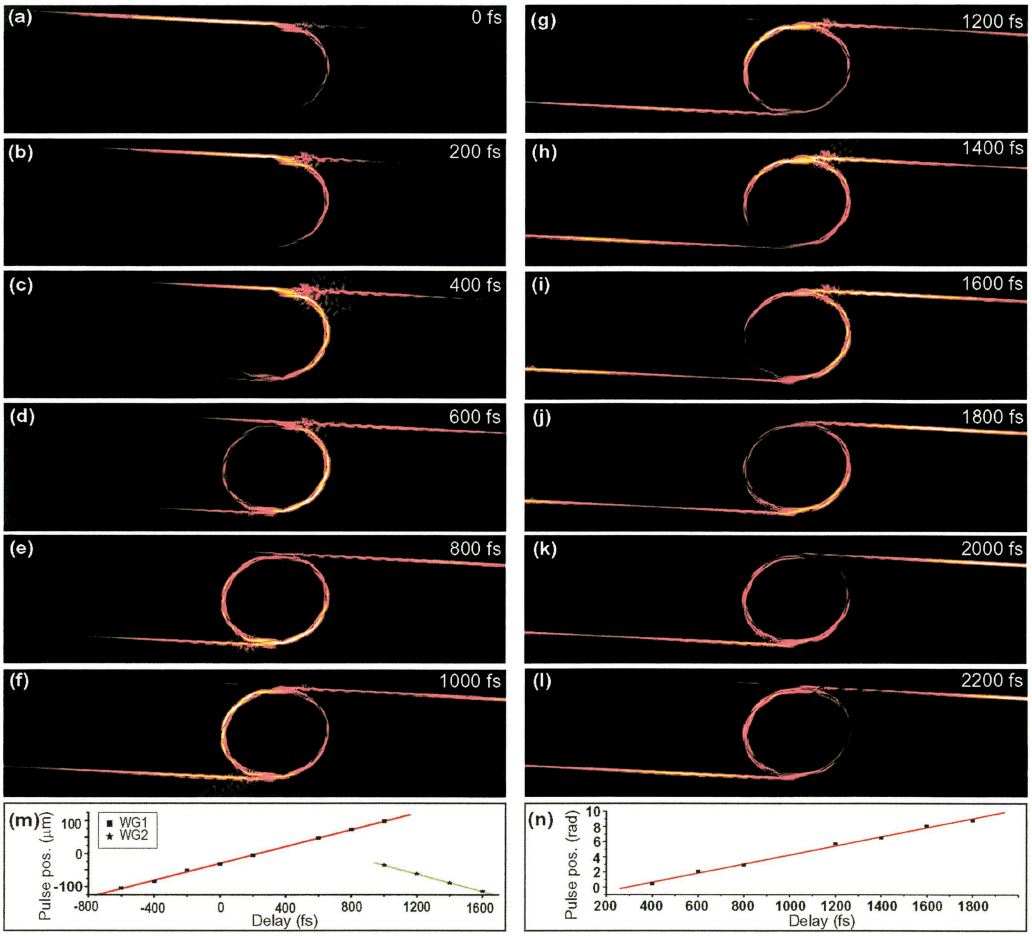

Fig. 3. (a)–(l) Sequence of snapshots in time of the measured optical amplitude on the low-finesse device (260.9 μm × 74.0 μm). The sequence clearly shows how a pulse couples into a resonator and couples out to the two adjacent waveguides at each round trip. (m) Position of the CoM of the pulse inside WG1 (red) and WG2 (green). (n) Angular position of the CoM of the pulse inside the resonator. The fitted slope directly yields an averaged angular group velocity inside the resonator of 6.0 ± 0.2 rad/ps, corresponding to 1.48×10^8 m/s.

This research is part of the strategic Research Orientation on Advanced Photonic Structures of the MESA+ Research Institute. Furthermore, this work is part of the research program of the Stichting voor Fundamenteel Onderzoek der Materie (FOM), which is financially supported by the Nederlandse Organisatie voor Wetenschappelijk Onderzoek. H. Gersen's e-mail address is h.gersen@tn.utwente.nl.

*Present address, FOM-institute for Atomic and Molecular Physics, Kruislaan 407, 1098 SJ Amsterdam, The Netherlands.

References

1. V. Sandoghdar, F. Treussart, J. Hare, V. Lefèvre-Seguin, J. M. Raimond, and S. Haroche, Phys. Rev. A **54,** 1777 (1996).
2. C. Gmachl, F. Capasso, E. E. Narimanov, J. U. Nöckel, A. D. Stone, J. Faist, D. L. Sivco, and A. Y. Cho, Science **280,** 1556 (1998).
3. K. J. Vahala, Nature **424,** 839 (2003).
4. S. C. Hagness, D. Rafizadeh, S. T. Ho, and A. Taflove, J. Lightwave Technol. **15,** 2154 (1997).
5. J. C. Knight, N. Dubreuil, V. Sandoghdar, J. Hare, V. Lefèvre-Sequin, J. M. Raimond, and S. Haroche, Opt. Lett. **21,** 698 (1996).
6. M. L. M. Balistreri, D. J. W. Klunder, F. C. Blom, A. Driessen, H. W. J. M. Hoekstra, J. P. Korterik, L. Kuipers, and N. F. van Hulst, Opt. Lett. **24,** 1829 (1999).
7. G. H. Vander Rhodes, B. B. Goldberg, M. S. Ünlü, S. T. Chu, and B. E. Little, IEEE J. Sel. Top. Quantum Electron. **6,** 46 (2000).
8. R. W. Shaw, W. B. Whitten, M. D. Barnes, and J. M. Ramsey, Opt. Lett. **23,** 1301 (1998).
9. J. P. Wolf, Y. L. Pan, G. M. Turner, M. C. Beard, C. A. Schmuttenmaer, S. Holler, and R. K. Chang, Phys. Rev. A **64,** 023808-1 (2001).
10. M. L. M. Balistreri, H. Gersen, J. P. Korterik, L. Kuipers, and N. F. van Hulst, Science **294,** 1080 (2001).
11. H. Gersen, J. P. Korterik, N. F. van Hulst, and L. Kuipers, Phys. Rev. E **68,** 026604-1 (2003).
12. D. J. W. Klunder, F. S. Tan, T. van der Veen, H. F. Bulthuis, G. Sengo, B. Docter, H. J. W. M. Hoekstra, and A. Driessen, J. Lightwave Technol. **LT21,** 1099 (2003).
13. B. E. Little, J. S. Foresi, G. Steinmeyer, E. R. Thoen, S. T. Chu, H. A. Haus, E. P. Ippen, L. C. Kimerling, and W. Greene, IEEE Photon. Technol. Lett. **10,** 549 (1998).
14. M. L. M. Balistreri, J. P. Korterik, L. Kuipers, and N. F. van Hulst, Phys. Rev. Lett. **85,** 294 (2000).